Nuclear Science and Techniques (2025) 36:220
https://doi.org/10.1007/s41365-025-01796-z

Study of shell evolution in neutron-rich boron, carbon, and nitrogen isotopes with in-medium similarity renormalization group calculations

Liu-Yuan Shen[1,2] · Qi Yuan[1,2] · Hong-Hui Li[1,2] · Meng-Ran Xie[1,2] · Jian-Guo Li[1,2] · Wei Zuo[1,2]

Received: 4 January 2025 / Revised: 17 March 2025 / Accepted: 31 March 2025 / Published online: 12 September 2025

Abstract

Neutron-rich boron, carbon, and nitrogen isotopes have garnered extensive experimental and theoretical interest. In the present work, we conducted a comprehensive study of these nuclei by utilizing *ab initio* valence-space in-medium similarity renormalization group calculations with chiral nucleon–nucleon and three-nucleon interactions. First, we systematically calculated the spectra of nuclei. Our results align well with the available experimental data, which are comparable to phenomenological shell model calculations. Subsequently, the evolution of the $N = 14$ and $N = 16$ shell gaps is discussed based on the calculated spectra and the effective single-particle energies. Our calculations suggest that the $N = 14$ neutron subshell is present in the oxygen isotopes but disappears in the boron, carbon, and nitrogen isotopic chains. Moreover, the $N = 16$ subshell is present in all isotopes but gradually decreases from ^{24}O to ^{21}B. These results provide valuable information for future studies.

Keywords *Ab initio* calculations · Chiral nuclear forces · Shell evolution · Low-lying spectra

1 Introduction

The shell structure of nuclei is a fundamental framework in nuclear physics. However, for neutron-rich nuclei far from the stability valley, the traditional magic numbers $N = 8, 20, 28$, and 40 vanish [1–10] and new magic numbers such as $N = 14$, 16, 32, and 34 emerged [11–14]. The evolution of shell structures in exotic nuclei has significantly deepened our understanding of nuclear quantum many-body systems and their underlying nuclear forces. Light neutron-rich nuclei are particularly intriguing, as the development of radioactive beam facilities has facilitated unprecedented exploration of isotopic chains extending to the dripline region [15].

The neutron-rich oxygen isotopes ^{22}O and ^{24}O are doubly magic nuclei with a high excitation energy of the first 2^+ excited state, providing clear evidence for the emergence of the $N = 14$ and 16 subshell closures [14, 16–18]. However, a comparison of the systematic behavior of the 2^+ energy levels in the oxygen and carbon isotopic chains suggests that the $N = 14$ shell gap disappears in the carbon isotopes [19, 20]. In ^{15}C, the ground state and first excited state are $1/2^+$ and $5/2^+$, respectively, indicating an inversion of the neutron $\nu 1s_{1/2}$ and $\nu 0d_{5/2}$ orbits in ^{15}C compared to ^{17}O [21, 22]. A similar inversion is anticipated when neutrons are added to ^{20}C [19, 20]. As the transition region between oxygen and carbon isotopes, nitrogen isotopes also signal the erosion of the $N = 14$ shell gap [23–26]. Moreover, the evolution of the $N = 16$ shell gap in neutron-rich boron, carbon, nitrogen, and oxygen isotopic chains remains an intriguing question. Further experimental and theoretical studies are required to fully understand the origin and evolution of $N = 14$ and $N = 16$ shell gaps.

Neutron-rich boron, carbon, and nitrogen isotopes exhibit many exotic phenomena. For instance, two-neutron halo structures were observed in ^{17}B [27], ^{19}B [28], and ^{22}C [29], while one-neutron halo structures were found in ^{15}C [30] and

This work was supported by the National Key R&D Program of China (Nos. 2024YFE0109800 and 2024YFE0109802), the National Natural Science Foundation of China (Nos. 12405141, 12347106, 12205340, and 12121005), the Gansu Natural Science Foundation (No. 25JRRA467), and the Key Research Program of the Chinese Academy of Sciences (No. XDPB15).

✉ Qi Yuan
yuanqi@impcas.ac.cn

[1] Institute of Modern Physics, Chinese Academy of Sciences, Lanzhou 730000, China

[2] School of Nuclear Science and Technology, University of Chinese Academy of Sciences, Beijing 100049, China

^{19}C [31]. In addition, the observation of the most neutron-rich unbound nuclei, ^{20}B and ^{21}B, was recently reported in Ref. [32]. Furthermore, a thick neutron skin has been detected in $^{17-22}$N [26]. These light neutron-rich systems, which straddle the neutron dripline, have accumulated a wealth of experimental data, thereby providing an ideal testing ground for theoretical models [33]. These studies have inspired extensive theoretical studies, including the shell model (SM) [21, 34–36], Gamow shell model (GSM) [37–39], antisymmetrized molecular dynamics (AMD) [40, 41], and *ab initio* no-core shell model (NCSM) calculations [42–44]. However, traditional SM calculations, which employ phenomenological interactions, have limited predictive power as the nuclei approach the dripline. In contrast, *ab initio* calculations based on high-resolution interactions derived from the chiral effective field theory (χEFT) of quantum chromodynamics have made great progress over the past decades [45–52], offering a more robust framework for understanding and predicting the properties of neutron-rich nuclei.

Systematic calculations of neutron-rich boron, carbon, and nitrogen isotopes enable us to gain a more comprehensive understanding of their exotic structures and shell evolution while simultaneously testing our *ab initio* methods and nuclear forces. Therefore, in this study, we performed systematic calculations of neutron-rich boron, carbon, and nitrogen isotopes using the *ab initio* valence-space in-medium similarity renormalization group (VS-IMSRG) [53–58] based on nucleon–nucleon (NN) and three-nucleon (3N) interactions derived from χEFT.

The remainder of this paper is organized as follows: First, we provide a brief introduction to the VS-IMSRG framework. Next, we present systematic calculations of the spectra of neutron-rich boron, carbon, and nitrogen isotopes. Subsequently, we discuss the shell evolution of the $N = 14$ and $N = 16$ shell gaps in these isotopes utilizing the calculated effective single-particle energies (ESPE). Finally, we conclude with a summary of this work.

2 Method

The intrinsic Hamiltonian of an A-nucleon system can be written as:

$$H = \sum_{i<j}^{A} \left(\frac{(\boldsymbol{p}_i - \boldsymbol{p}_j)^2}{2mA} + v_{ij}^{\mathrm{NN}} \right) + \sum_{i<j<k}^{A} v_{ijk}^{\mathrm{3N}}, \tag{1}$$

where $\boldsymbol{p}$ is the nucleon momentum in the laboratory, m is the nucleon mass, v^{NN} and v^{3N} are the NN and 3N interactions, respectively. In this study, we used three different χEFT NN + 3N interactions: EM1.8/2.0 [59, 60], N^{3}LO+3N(lnl) [9, 61] and N^{4}LO+3N(lnl) [62]. The EM1.8/2.0 interaction, consisting of a next-to-next-to-next-to-leading order (N^{3}LO) NN interaction softened by the similarity renormalization group (SRG) evolution with momentum resolution scale $\lambda = 1.8\,\mathrm{fm}^{-1}$ and a next-to-next-to-leading order (N^{2}LO) 3N interaction with momentum cutoff $\Lambda = 2.0\,\mathrm{fm}^{-1}$, can reproduce well the ground-state energies up to ^{132}Sn [59, 60]. The N^{3}LO+3N(lnl) interaction, which presents good description of ground-state energies up to nickel isotopes, is composed of an N^{3}LO NN interaction and an N^{2}LO 3N interaction, adopting a large SRG scale of $\lambda = 2.6\,\mathrm{fm}^{-1}$ for the NN interaction without including the induced 3N force [9, 61]. The N^{4}LO+3N(lnl) interaction, composed of a next-to-next-to-next-to-next-to-leading order (N^{4}LO) NN interaction and an N^{2}LO 3N interaction, also adopts a large SRG scale of $\lambda = 2.6\,\mathrm{fm}^{-1}$ for the NN interaction, without including the induced 3N force [62]. In this study, we take a harmonic-oscillator basis at $\hbar\omega = 16$ MeV with $e_{\max} = 2n + l = 14$ and $E_{3\max} = 14$, which is sufficiently large for convergence.

In practical calculations, Hamiltonian (1) is rewritten as normal-order operators with respect to the Hartree–Fock reference state,

$$\begin{aligned} H = E_0 + \sum_{ij} f_{ij} : a_i^\dagger a_j : + \frac{1}{4} \sum_{ijkl} \Gamma_{ijkl} : a_i^\dagger a_j^\dagger a_l a_k : \\ + \frac{1}{36} \sum_{ijklmn} W_{ijklmn} : a_i^\dagger a_j^\dagger a_k^\dagger a_n a_m a_l :, \end{aligned} \tag{2}$$

where E_0, f, Γ, W refer to the normal-ordered zero-, one-, two- and three-body terms, respectively. Because the contribution of 3N force can be captured well at the normal-ordered two-body level [63], the residual normal-ordered three-body term W is neglected.

Next, using the continuous unitary transformation $U(s)$, the Hamiltonian (2) is decoupled from the large Hilbert space to a small valence space using VS-IMSRG. This is achieved by solving the flow equation,

$$\frac{\mathrm{d}H(s)}{\mathrm{d}s} = [\eta(s), H(s)], \tag{3}$$

with an anti-Hermitian generator,

$$\eta(s) \equiv \frac{dU(s)}{ds} U^\dagger(s) = -\eta^\dagger(s). \tag{4}$$

In the present study, we adopted protons in the p shell and neutrons in the sd shell as the valence space. In practical calculations, the Magnus formalism is employed with all operators truncated at the two-body level [64]. The effective Hamiltonians for this model space are consistently derived by VS-IMSRG with ensemble normal ordering (ENO) [55]. Then, we use the large-scale shell model code KSHELL [65] to diagonalize the effective Hamiltonians.

3 Results

3.1 Energy spectra

Nuclear spectra provide invaluable insights into nuclear structure. In this study, the spectra of neutron-rich boron, carbon, and nitrogen isotopes were systematically calculated using *ab initio* VS-IMSRG with three sets of χEFT NN + 3N interactions, that is, EM1.8/2.0 [59, 60], N^{3}LO+3N(lnl) [9, 61], and N^{4}LO+3N(lnl) [62]. For comparison, we also performed phenomenological SM calculations using the YSOX interaction within the full *psd* valence space, which accurately reproduced the properties of boron, carbon, nitrogen, and oxygen isotopes [34]. The results were compared with the available experimental data, as illustrated in Figs. 1, 2, and 3.

Nitrogen isotopes have abundant experimental data, which provide a valuable test ground for our *ab initio* calculations. In addition, nitrogen nuclei lie between oxygen and carbon isotopes, offering essential insights into the shell evolution. For ^{16}N, the ordering of the first four states is experimentally determined as 2^-, 0^-, 3^-, and 1^- [66]. Our VS-IMSRG calculations with the EM1.8/2.0 and N^{3}LO+3N(lnl) interactions showed good agreement with the experimental results, whereas the SM calculations using the YSOX interaction failed to reproduce the spectra of ^{16}N. For ^{17}N, the VS-IMSRG calculations with the three NN + 3N interactions as well as the SM calculations using the YSOX interaction reproduced the lowest three states well. In the case of ^{18}N, the ground state was correctly reproduced by the VS-IMSRG calculations with the EM1.8/2.0 interaction and the SM calculations using the YSOX interaction. However, the VS-IMSRG calculations with N^{3}LO+3N(lnl)

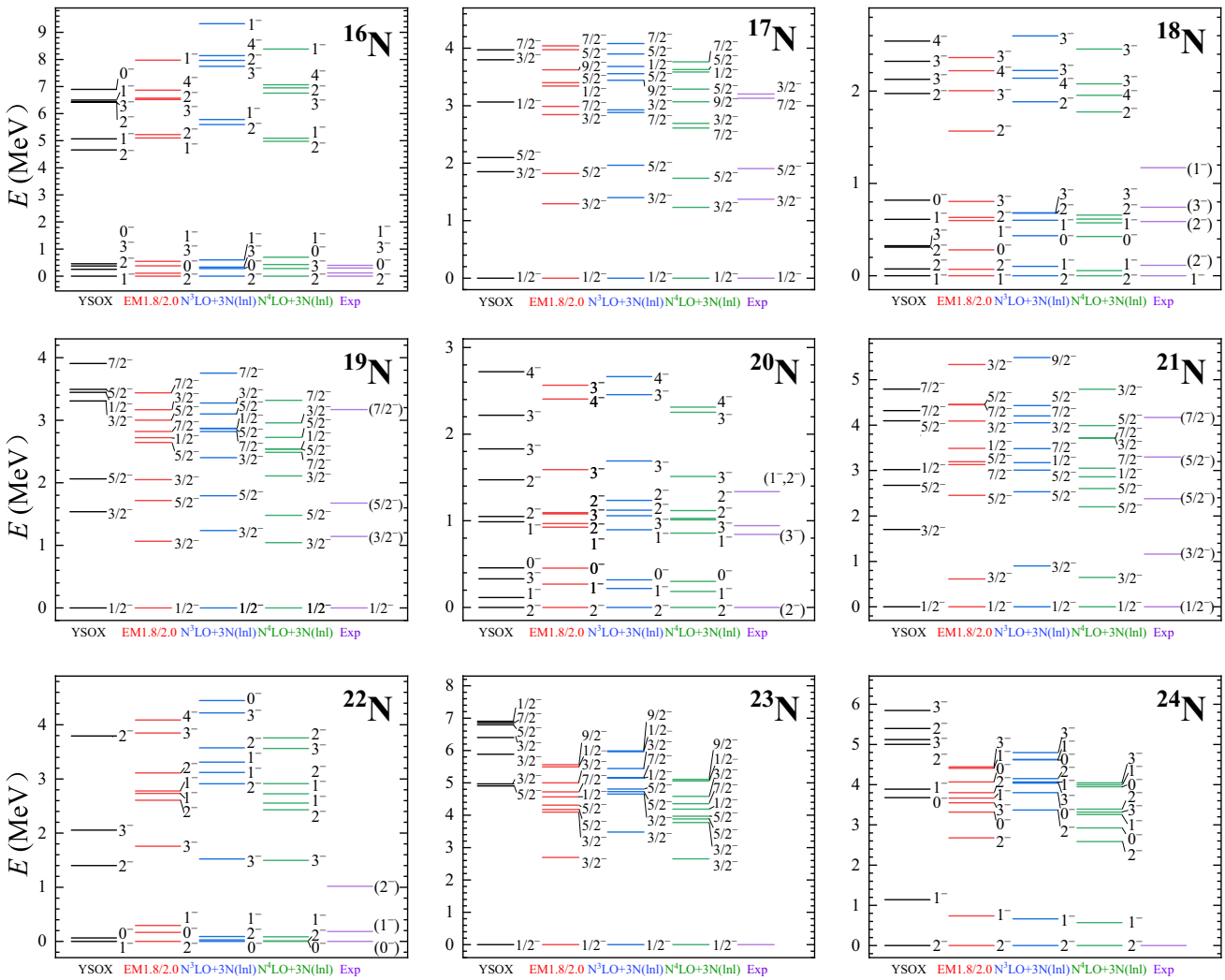

Fig. 1 Energy spectra of $^{16-24}$N calculated by *ab initio* VS-IMSRG using the EM1.8/2.0, N^{3}LO+3N(lnl), and N^{4}LO+3N(lnl) interactions, compared with the SM calculations using the YSOX interaction and the available experimental data [66]

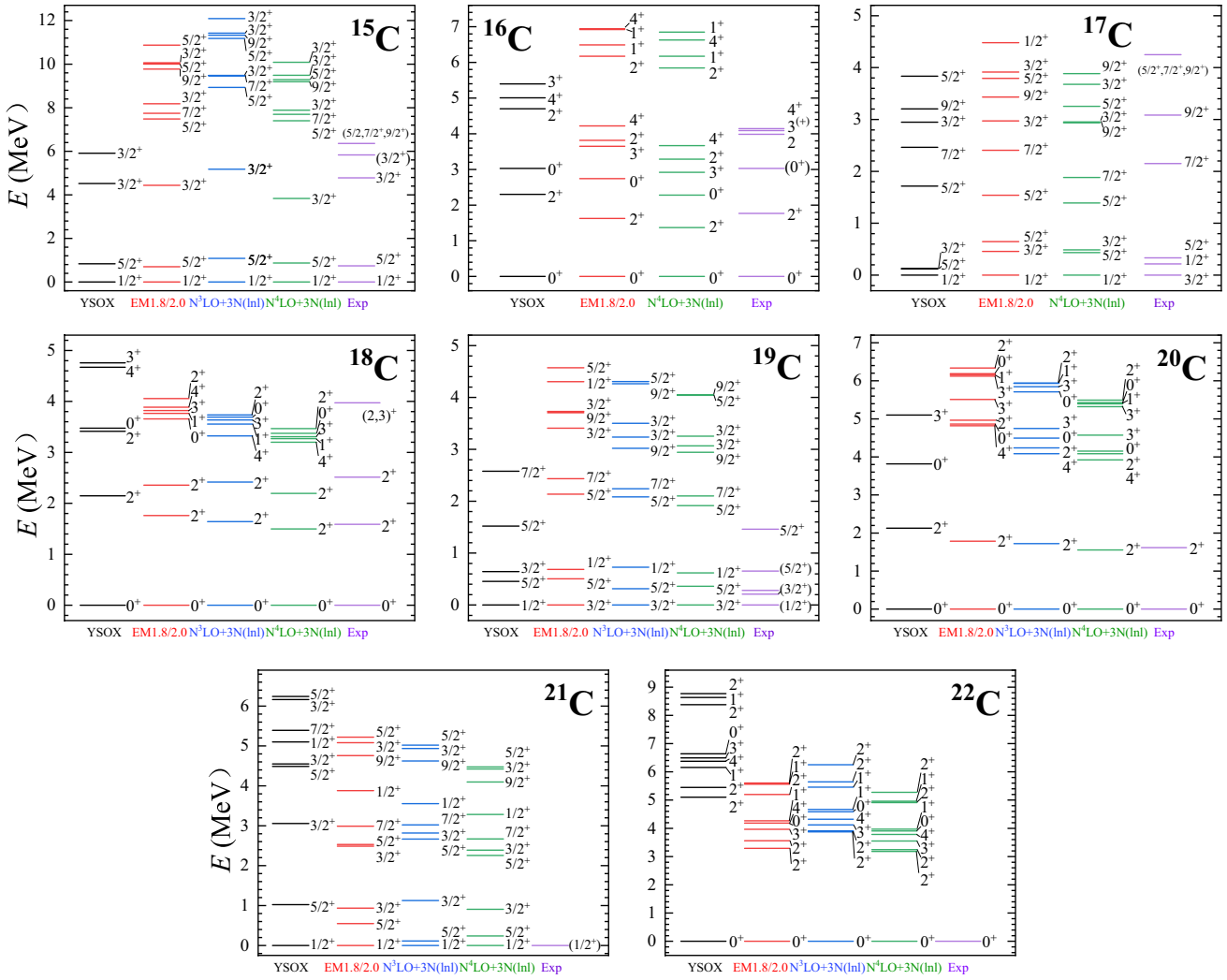

Fig. 2 Energy spectra of $^{15-22}$C calculated by *ab initio* VS-IMSRG using the EM1.8/2.0, N^{3}LO+3N(lnl), and N^{4}LO+3N(lnl) interactions, compared with the SM calculations using the YSOX interaction and the available experimental data [66]

and N^{4}LO+3N(lnl) interactions give 2^- as the ground state. For ^{19,21}N, all calculations correctly gave the ground state as $1/2^-$ and predicted the first excited state as $3/2^-$, with the excited states yet to be experimentally confirmed. For ^{20}N, the ground state is 2^- given by all calculations. In the case of ^{22}N, the VS-IMSRG calculations with the N^{3}LO+3N(lnl) and N^{4}LO+3N(lnl) interactions predicted a 0^- ground state, whereas the VS-IMSRG calculations with the EM1.8/2.0 interaction and the SM calculations using the YSOX interaction predicted the ground state to be 2^- and 1^-, respectively. The size of the $N = 16$ shell gap in ^{23}N remains unclear [67]. All calculations predicted the ground state of ^{23}N to be $1/2^-$. However, the SM calculations with the YSOX interaction yielded higher excitation spectra than the VS-IMSRG results, indicating an overly large $N = 16$ shell gap in the SM calculations using the YSOX interaction. This behavior was also observed in ^{21}B, ^{22}C, and ^{24}O, as discussed above. For ^{24}N, all the calculations give the ground state as 2^- and predict the first excited state as 1^-.

Neutron-rich carbon isotopes have attracted considerable experimental and theoretical attention. The ground state and first excited state of ^{15}C are $1/2^+$ and $5/2^+$, respectively, indicating an inversion of the neutron $\nu 1s_{1/2}$ and $\nu 0d_{5/2}$ orbits in carbon isotopes [21, 22]. Our VS-IMSRG calculations, along with the SM calculations, accurately reproduced the spectra of ^{15}C. The VS-IMSRG calculations with the N^{3}LO+3N(lnl) interaction for ^{16,17}C did not converge; therefore, we only present the results for ^{16,17}C using the EM1.8/2.0 and N^{4}LO+3N(lnl) interactions in Fig. 2. For ^{16,18,20}C, the first 2^+ excited states obtained from our VS-IMSRG calculations are in good agreement with the experimental data, whereas SM calculations using the YSOX interaction generally provide

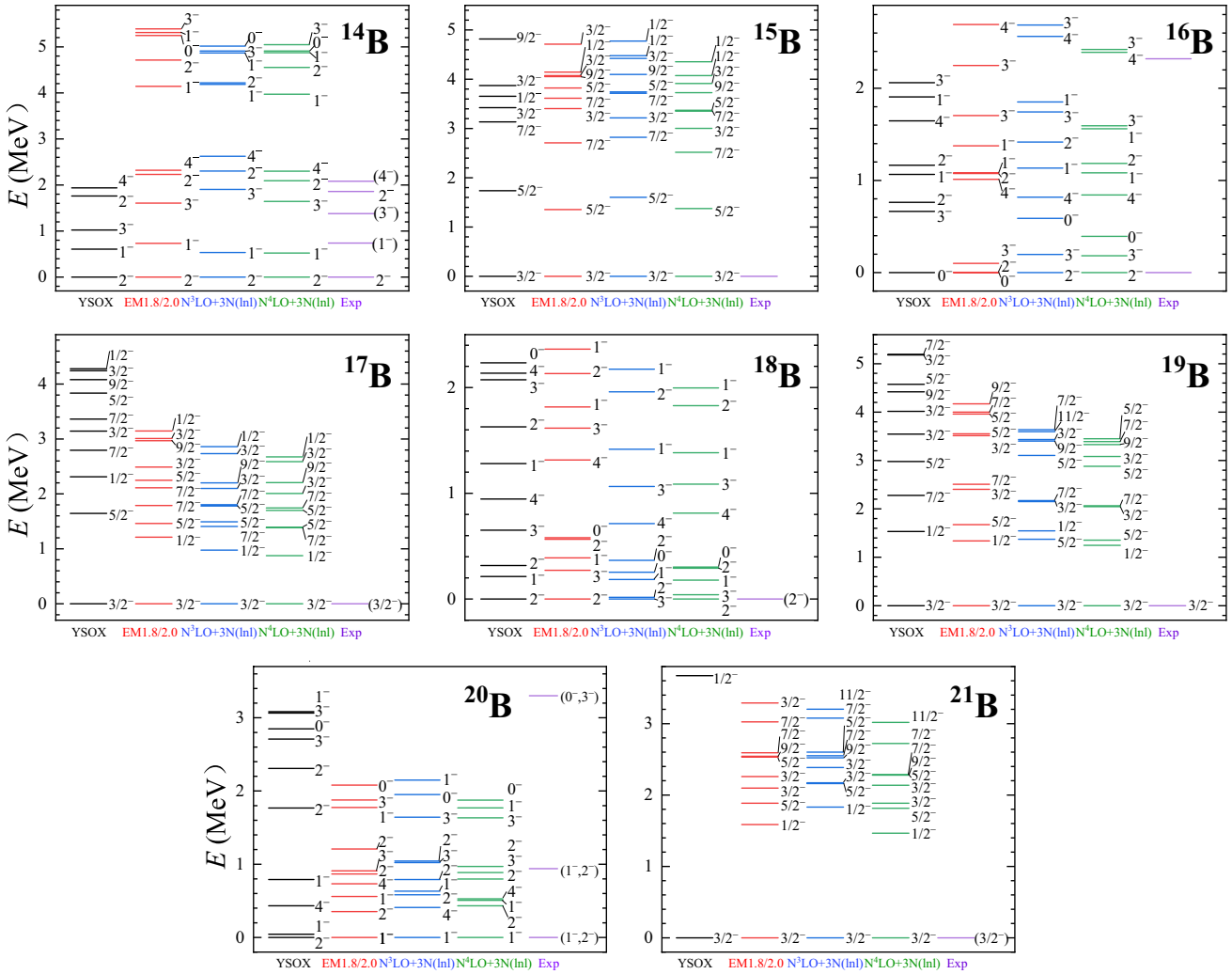

Fig. 3 Energy spectra of $^{14-21}$B calculated by *ab initio* VS-IMSRG using the EM1.8/2.0, N^{3}LO+3N(lnl), and N^{4}LO+3N(lnl) interactions, compared with the SM calculations using the YSOX interaction and the available experimental data [66]

higher energies for the first 2^+ excited states of these nuclei. In particular, for ^{22}C, the energy of the first 2^+ excited state calculated by SM using the YSOX interaction is significantly higher than that predicted by VS-IMSRG. Notably, the first 2^+ excited state of ^{24}O, calculated by SM with YSOX interaction, is 5.41 MeV, which is higher than the experimental value of 4.76 MeV. In contrast, our VS-IMSRG calculations with the EM1.8/2.0, N^{3}LO+3N(lnl), and N^{4}LO+3N(lnl) interactions give the first 2^+ excited state of ^{24}O to be 4.87, 5.26, and 4.39 MeV, respectively, which are in better agreement with the experimental value. Moreover, the first 2^+ excited state of ^{22}C calculated by VS-IMSRG is significantly higher than that of the neighboring carbon isotopes, implying the presence of the $N = 16$ shell gap in ^{22}C. However, the calculated first 2^+ excited state of ^{22}C is lower than that of ^{24}O, suggesting a reduction in the $N = 16$ shell gap in ^{22}C compared to ^{24}O. In addition, the low energy of the first 2^+ excited state in ^{20}C indicates the disappearance of the $N = 14$ shell gap in ^{20}C [19]. For ^{17}C and ^{19}C, our VS-IMSRG calculations failed to reproduce the experimental spectra because of the absence of continuum coupling in the current method, as discussed in Ref. [37, 68].

In the case of neutron-rich boron isotopes, experimental data are limited. For ^{14}B, the ordering of the first five states is experimentally assigned as 2^-, 1^-, 3^-, 2^-, and 4^- [66]. Our *ab initio* VS-IMSRG calculations with the three NN + 3N interactions as well as the SM calculations using the YSOX interaction are all in good agreement with the experimental results. The spin and parity of the ground state for isotopes heavier than ^{14}B have not yet been confirmed experimentally. For ^{15,17,19,21}B, our VS-IMSRG calculations with the three NN + 3N interactions predict that the ground states of these isotopes are all $3/2^-$, which is

consistent with SM calculations using the YSOX interaction. For ^{16}B, the VS-IMSRG calculations with the N^{3}LO+3N(lnl) and N^{4}LO+3N(lnl) interactions predict the ground state to be 2^-, whereas the VS-IMSRG calculations with the EM1.8/2.0 interaction predict a ground state of 0^- with a 2^- excited state that is nearly degenerate. In addition, the ground state of ^{16}B obtained from the SM calculations using the YSOX interaction is also 0^-. For the unbound nucleus ^{18}B, SM calculations using YSOX and WBP [69] interactions predicted the ground state to be 2^-. Our VS-IMSRG calculations with the EM1.8/2.0 and N^{4}LO+3N(lnl) interactions also predicted the ground state of ^{18}B to be 2^-, but the VS-IMSRG calculations with the N^{3}LO+3N(lnl) interaction gave the ground state of ^{18}B to be 3^-. Both ^{20}B and ^{21}B are unbound nuclei that exist as resonances and decay via one- or two-neutron emissions [32]. For ^{20}B, our VS-IMSRG calculations with the three NN + 3N interactions predict the ground state to be 1^-, whereas SM calculations using the YSOX interaction yield the ground state 2^-. For ^{21}B, our VS-IMSRG calculations with the three NN + 3N interactions predicted a significantly lower energy for the first excited state $1/2^-$ compared to the SM calculations using the YSOX interaction, a situation similar to that observed for ^{22}C and ^{24}O above. The $1/2^-$ state of ^{21}B calculated with VS-IMSRG has larger neutron excitation components than those in the SM calculations. However, the subsequent analysis of the ESPE calculated by VS-IMSRG suggests that the $N = 16$ subshell still exists in ^{21}B.

Overall, our *ab initio* VS-IMSRG calculations based on the three χEFT NN + 3N interactions, particularly the EM1.8/2.0 interaction, were in good agreement with the available experimental data. These results provide critical assistance for future research.

3.2 Shell evolution

In neutron-rich boron, carbon, nitrogen, and oxygen isotopes, the evolution of $N = 14$ and $N = 16$ shell gaps has attracted significant experimental and theoretical attention. The ESPE provides a good reflection of the size of shell gaps, which defined as [70, 71]

$$\varepsilon_i = \varepsilon_i^{\text{core}} + \sum_j n_j V_{ij}^m, \tag{5}$$

where $\varepsilon_i^{\text{core}}$ is the valence-space single-particle energy, V^m is the monopole interaction, and n_j is the occupation number calculated consistently using the SM.

To study the evolution of the $N = 14$ and $N = 16$ shell gaps, we calculated the ESPE of the $\nu 1s_{1/2}$, $\nu 0d_{5/2}$, and $\nu 0d_{3/2}$ orbits in these nuclei employing the VS-IMSRG method, based on the EM1.8/2.0, N^{3}LO+3N(lnl), and N^{4}LO+3N(lnl) interactions, compared with the SM calculations using the YSOX interaction. As shown in Fig. 4, for the VS-IMSRG calculations, when protons are removed from the oxygen isotopes, the ESPE of the $\nu 1s_{1/2}$ orbital is gradually lowered relative to the $\nu 0d_{5/2}$ orbital, and a reversal occurs in the boron and carbon isotopes. This indicates that the $N = 14$ neutron subshell is present in the oxygen isotopes but disappears in the boron, carbon, and nitrogen isotopic chains. The SM calculations using the YSOX interaction show the same trend as the VS-IMSRG results, whereas the $N = 14$ shell gaps in ^{21}N and ^{22}O calculated by SM are significantly larger than those obtained from VS-IMSRG. Notably, the $N = 16$ subshell is present in the boron, carbon, nitrogen, and oxygen isotopic chains and gradually decreases from ^{24}O to ^{21}B. Moreover, the $N = 16$ shell gap calculated by SM using the YSOX interaction was significantly larger than that calculated by VS-IMSRG. Additionally, the $N = 16$ shell gap calculated by VS-IMSRG using the N^{3}LO+3N(lnl) interaction is generally larger than that calculated using the EM1.8/2.0 and N^{4}LO+3N(lnl) interactions. Correspondingly, the energy spectra exhibited higher excitation energies, particularly in ^{24}O, as discussed above.

To further understand the contribution of the 3N force to the shell evolution, Fig. 5 shows the VS-IMSRG calculations using the full NN + 3N EM1.8/2.0 interaction (solid lines) compared with the VS-IMSRG calculations without the 3N force (dashed lines). As shown in Fig. 5, the 3N force enhances the $N = 14$ shell gap in the oxygen isotopes while reducing the $N = 16$ shell gap in the boron, carbon, nitrogen, and oxygen isotopes. A similar

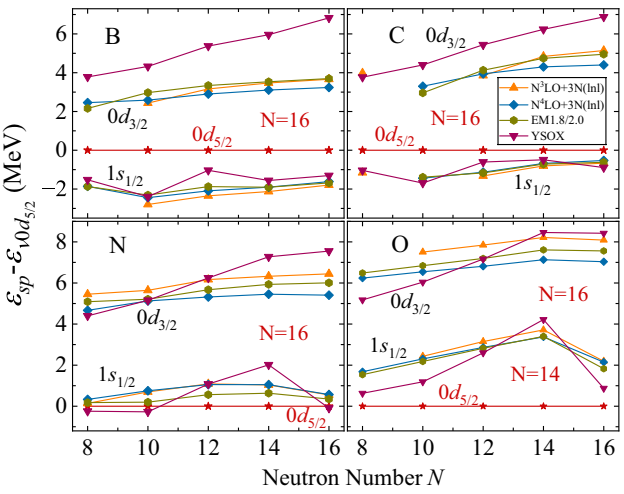

Fig. 4 ESPEs relative to the neutron $\nu 0d_{5/2}$ orbital in boron, carbon, nitrogen, and oxygen isotopes, calculated by VS-IMSRG using the EM1.8/2.0, N^{3}LO+3N(lnl) and N^{4}LO+3N(lnl) interactions, respectively, compared with the SM calculations using the YSOX interaction

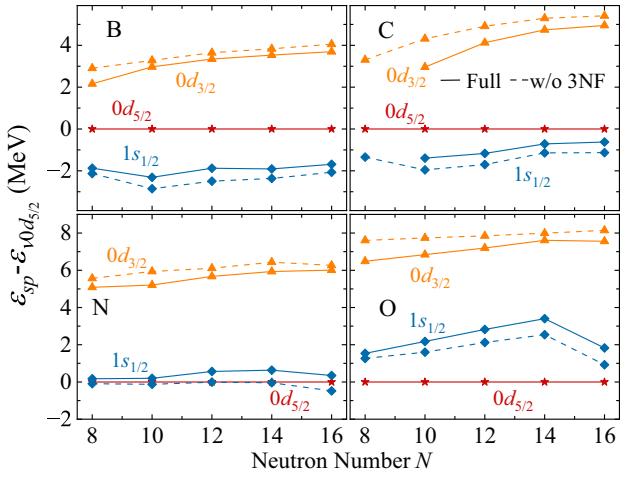

Fig. 5 ESPEs relative to the neutron $\nu 0d_{5/2}$ orbital in boron, carbon, nitrogen, and oxygen isotopes, calculated by VS-IMSRG with the full NN + 3N EM1.8/2.0 interaction (solid lines), compared to the results obtained without the 3N force included (dashed lines)

trend was observed for the results using N^{3}LO+3N(lnl) and N^{4}LO+3N(lnl) interactions.

To analyze the roles of different components of the interaction in shell evolution, we employed the spin-tensor decomposition method [72–74] to decompose the effective interaction derived from VS-IMSRG into central, tensor, and spin-orbit (LS) parts. First, we conducted systematic calculations for boron isotopes and compared the contributions of different components of the interaction derived from VS-IMSRG across three sets of χEFT NN + 3N interactions: N^{3}LO+3N(lnl), N^{4}LO+3N(lnl), and EM1.8/2.0. We also compared the results with the SM calculations using the YSOX interaction. As shown in Fig. 6, the solid lines represent the results with the full interaction, the dashed lines represent the results without the contribution of the tensor force, and the dot-dashed lines represent the results without the contribution of the two-body LS part. In our VS-IMSRG calculations, we can see that the tensor force slightly lowers the ESPE of the $\nu 0d_{3/2}$ orbital relative to the $\nu 0d_{5/2}$ orbital, whereas the two-body LS component increases the ESPE of both the $\nu 0d_{3/2}$ and $\nu 1s_{1/2}$ orbits relative to the $\nu 0d_{5/2}$ orbital. Moreover, the contributions of the tensor force and the two-body LS part were similar across the three sets of NN + 3N forces. Additionally, SM calculations using the YSOX interaction demonstrated the same trend as the VS-IMSRG results, although the strength of the tensor force and the two-body LS force showed minor differences. Next, we present the contributions of the different components of the interactions in various isotopes. For clarity, we only show the results calculated by VS-IMSRG using the EM1.8/2.0 interaction. In Fig. 7, the solid and dashed lines represent the ESPE with and without the contribution of the tensor force, respectively. It can be seen that the tensor force only slightly reduces the $N = 16$ shell gap for all the isotopes. Figure 8 compares the results obtained with and without the two-body LS part. The two-body LS part significantly lowers the ESPE of the $\nu 0d_{5/2}$ orbital and causes inversion of the $\nu 1s_{1/2}$ and $\nu 0d_{5/2}$ orbits in oxygen isotopes compared to boron and carbon isotopes. This inversion is the origin of the $N = 14$ shell gap in the oxygen isotopes. In addition, the two-body LS part significantly increases the ESPE of the $\nu 0d_{3/2}$ orbital, leading to the appearance of the $N = 16$ subshell.

In Ref. [4], the inversion between the neutron $\nu 1s_{1/2}$ and $\nu 0d_{5/2}$ orbits in ^{15}C and ^{17}O is depicted by analyzing the monopole matrix elements of the YSOX interaction, assuming that, from ^{15}C to ^{17}O, the proton $\pi 0p_{1/2}$ orbit is fully occupied, and the last neutron is in either the $\nu 1s_{1/2}$ or $\nu 0d_{5/2}$ orbital. Similar to the discussion in Refs. [4], we extracted the contributions of the monopole

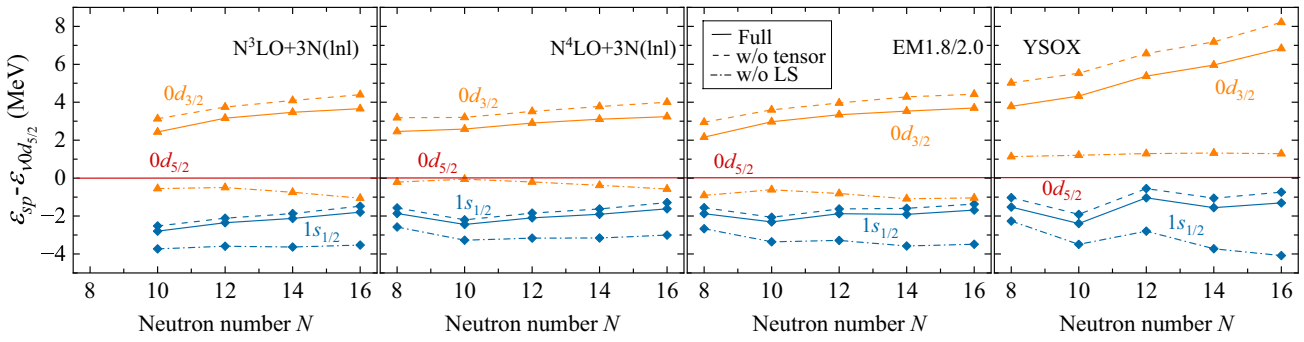

Fig. 6 ESPEs relative to the neutron $\nu 0d_{5/2}$ orbital in boron isotopes, calculated by VS-IMSRG using the N^{3}LO+3N(lnl), N^{4}LO+3N(lnl), and EM1.8/2.0 interactions with (solid lines) and without the contribution of the tensor force (dashed lines)/LS force (dot-dashed lines), as well as the SM calculations using the YSOX interaction

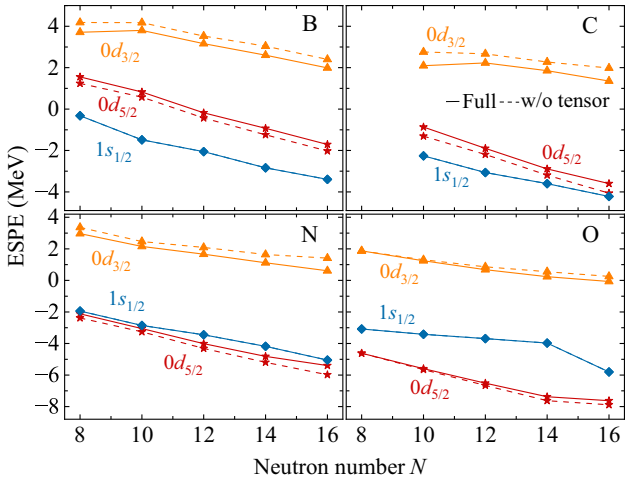

Fig. 7 ESPEs of the neutron $\nu 1s_{1/2}$, $\nu 0d_{5/2}$, and $\nu 0d_{3/2}$ orbits in boron, carbon, nitrogen, and oxygen isotopes, calculated by VS-IMSRG using the EM1.8/2.0 interaction with (solid lines) and without (dashed lines) the contribution of the tensor force

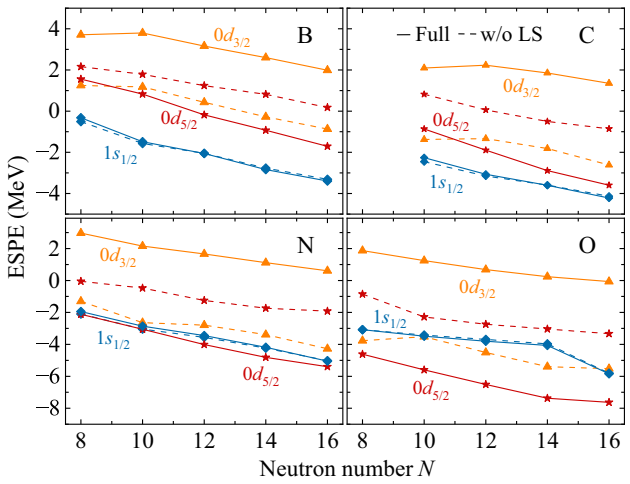

Fig. 8 ESPEs of the neutron $\nu 1s_{1/2}$, $\nu 0d_{5/2}$, and $\nu 0d_{3/2}$ orbits in boron, carbon, nitrogen, and oxygen isotopes, calculated by VS-IMSRG using the EM1.8/2.0 interaction with (solid lines) and without (dashed lines) the contribution of the spin-orbit (LS) force

matrix elements from various components of the effective interaction derived by VS-IMSRG, including the central, tensor, and LS parts, as shown in Fig. 9. Here, the rest is due to the Adependence of the Hamiltonian. The two-body LS part significantly contributes to the shift of the $\nu 1s_{1/2}$ orbital relative to the $\nu 0d_{5/2}$ orbital, even when determining the inversion of the $\nu 1s_{1/2}$ and $\nu 0d_{5/2}$ orbits. In contrast,

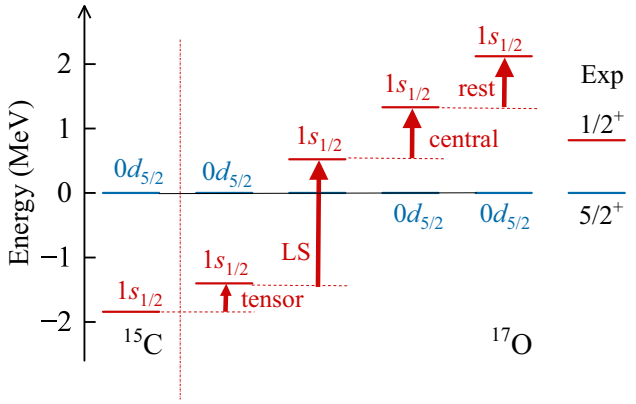

Fig. 9 ESPEs of the neutron $\nu 1s_{1/2}$ orbit relative to the $\nu 0d_{5/2}$ orbit in ^{15}C and ^{17}O, calculated by VS-IMSRG with the EM1.8/2.0 interaction. The contributions of the tensor, LS, and central forces to the ESPE were decomposed. The rest part is due to our Hamiltonian is A-dependent

the contribution from the tensor force was much smaller than that observed in the YSOX interaction in Ref. [4].

4 Conclusion

Utilizing three sets of chiral NN + 3N interactions, EM1.8/2.0, N^{3}LO+3N(lnl), and N^{4}LO+3N(lnl), we present *ab initio* VS-IMSRG calculations for neutron-rich boron, carbon, and nitrogen isotopes. We systematically calculated and predicted the low-lying spectra of these nuclei. For comparison, we also performed SM calculations using the YSOX interaction. Based on the calculated spectra and effective single-particle energies, we studied the evolution of $N = 14$ and $N = 16$ shell gaps. Our results suggest that the $N = 14$ neutron subshell is present in the oxygen isotopes but collapses in the boron, carbon, and nitrogen isotopic chains. Furthermore, the $N = 16$ subshell is predicted to be present in boron, carbon, nitrogen, and oxygen isotopes, but its size gradually decreases from ^{24}O to ^{21}B. Additionally, we investigated the roles of the different components of the interaction in shell evolution by employing the spin-tensor decomposition method. We find that the two-body spin-orbit force plays a significant role in the formation of the $N = 14$ and $N = 16$ shell gaps. In general, our *ab initio* VS-IMSRG calculations agree well with the available experimental data, and theoretical predictions for these nuclei will be helpful for future experiments.

Author contributions All authors contributed to the study conception and design. Material preparation, data collection and analysis were performed by Liu-Yuan Shen, Qi Yuan, Hong-Hui Li, and Jian-Guo Li. The first draft of the manuscript was written by Liu-Yuan Shen, and all authors commented on previous versions of the manuscript. All authors read and approved the final manuscript.

Data availability The data that support the findings of this study are openly available in Science Data Bank at https://cstr.cn/31253.11.sciencedb.j00186.00758 and https://www.doi.org/10.57760/sciencedb.j00186.00758.

Declarations

Conflict of interest The authors declare that they have no Conflict of interest.

References

1. E.K. Warburton, J.A. Becker, B.A. Brown, Mass systematics for A=29–44 nuclei: the deformed A∼32 region. Phys. Rev. C **41**, 1147–1166 (1990). https://doi.org/10.1103/PhysRevC.41.1147
2. E. Caurier, G. Martínez-Pinedo, F. Nowacki et al., The shell model as a unified view of nuclear structure. Rev. Mod. Phys. **77**, 427–488 (2005). https://doi.org/10.1103/RevModPhys.77.427
3. O. Sorlin, M.G. Porquet, Nuclear magic numbers: new features far from stability. Prog. Part. Nucl. Phys. **61**, 602–673 (2008). https://doi.org/10.1016/j.ppnp.2008.05.001
4. T. Otsuka, A. Gade, O. Sorlin et al., Evolution of shell structure in exotic nuclei. Rev. Mod. Phys. **92**, 015002 (2020). https://doi.org/10.1103/RevModPhys.92.015002
5. H. Iwasaki, A. Dewald, C. Fransen et al., Low-lying neutron intruder state in ^{13}B and the fading of the $N = 8$ shell closure. Phys. Rev. Lett. **102**, 202502 (2009). https://doi.org/10.1103/PhysRevLett.102.202502
6. M. Mougeot, D. Atanasov, K. Blaum et al., Precision mass measurements of $^{58-63}$Cr: nuclear collectivity towards the $N = 40$ island of inversion. Phys. Rev. Lett. **120**, 232501 (2018). https://doi.org/10.1103/PhysRevLett.120.232501
7. C. Force, S. Grévy, L. Gaudefroy et al., Prolate-spherical shape coexistence at $N = 28$ in ^{44}S. Phys. Rev. Lett. **105**, 102501 (2010). https://doi.org/10.1103/PhysRevLett.105.102501
8. H.L. Crawford, R.M. Clark, P. Fallon et al., Quadrupole collectivity in neutron-rich Fe and Cr isotopes. Phys. Rev. Lett. **110**, 242701 (2013). https://doi.org/10.1103/PhysRevLett.110.242701
9. Q. Yuan, J.G. Li, H.H. Li, *Ab initio* calculations for well deformed nuclei: ^{40}Mg and ^{42}Si. Phys. Lett. B **848**, 138331 (2024). https://doi.org/10.1016/j.physletb.2023.138331
10. Q. Yuan, J.G. Li, W. Zuo, Ab initio calculations for configuration-coexisting states in ^{45}S: an extension from ^{43}S. Phys. Rev. C **109**, L041301 (2024). https://doi.org/10.1103/PhysRevC.109.L041301
11. F. Wienholtz, D. Beck, K. Blaum et al., Masses of exotic calcium isotopes pin down nuclear forces. Nature **498**, 346 (2013). https://doi.org/10.1038/nature12226
12. D. Steppenbeck, S. Takeuchi, N. Aoi et al., Evidence for a new nuclear 'magic number' from the level structure of ^{54}Ca. Nature **502**, 207 (2013). https://doi.org/10.1038/nature12522
13. W.F. Rogers, S. Garrett, A. Grovom et al., Unbound excited states of the $N = 16$ closed shell nucleus ^{24}O. Phys. Rev. C **92**, 034316 (2015). https://doi.org/10.1103/PhysRevC.92.034316
14. E. Becheva, Y. Blumenfeld, E. Khan et al., $N = 14$ shell closure in ^{22}O viewed through a neutron sensitive probe. Phys. Rev. Lett. **96**, 012501 (2006). https://doi.org/10.1103/PhysRevLett.96.012501
15. W. Liu, J.L. Lou, Y.L. Ye et al., Experimental study of intruder components in light neutron-rich nuclei via single-nucleon transfer reaction. Nucl. Sci. Tech. **31**, 20 (2020). https://doi.org/10.1007/s41365-020-0731-y
16. M. Stanoiu, F. Azaiez, Z. Dombrádi et al., $N = 14$ and 16 shell gaps in neutron-rich oxygen isotopes. Phys. Rev. C **69**, 034312 (2004). https://doi.org/10.1103/PhysRevC.69.034312
17. R. Kanungo, C. Nociforo, A. Prochazka et al., One-neutron removal measurement reveals ^{24}O as a new doubly magic nucleus. Phys. Rev. Lett. **102**, 152501 (2009). https://doi.org/10.1103/PhysRevLett.102.152501
18. K. Tshoo, Y. Satou, H. Bhang et al., $N = 16$ spherical shell closure in ^{24}O. Phys. Rev. Lett. **109**, 022501 (2012). https://doi.org/10.1103/PhysRevLett.109.022501
19. M. Stanoiu, D. Sohler, O. Sorlin et al., Disappearance of the $N = 14$ shell gap in the carbon isotopic chain. Phys. Rev. C **78**, 034315 (2008). https://doi.org/10.1103/PhysRevC.78.034315
20. M.J. Strongman, A. Spyrou, C.R. Hoffman et al., Disappearance of the $N = 14$ shell. Phys. Rev. C **80**, 021302 (2009). https://doi.org/10.1103/PhysRevC.80.021302
21. C.X. Yuan, C. Qi, F.R. Xu, Shell evolution in neutron-rich carbon isotopes: unexpected enhanced role of neutron-neutron correlation. Nucl. Phys. A **883**, 25–34 (2012). https://doi.org/10.1016/j.nuclphysa.2012.04.003
22. J. Lois-Fuentes, B. Fernández-Domínguez, X. Pereira-López et al., Cross-shell states in ^{15}C: a test for p-sd interactions. Phys. Lett. B **845**, 138149 (2023). https://doi.org/10.1016/j.physletb.2023.138149
23. D. Sohler, M. Stanoiu, Z. Dombrádi et al., In-beam γ-ray spectroscopy of the neutron-rich nitrogen isotopes $^{19-22}$N. Phys. Rev. C **77**, 044303 (2008). https://doi.org/10.1103/PhysRevC.77.044303
24. Z. Elekes, Z. Vajta, Z. Dombrádi et al., Nuclear structure study of ^{19,21}N nuclei by γ spectroscopy. Phys. Rev. C **82**, 027305 (2010). https://doi.org/10.1103/PhysRevC.82.027305
25. C. Rodríguez-Tajes, D. Cortina-Gil, H. Álvarez-Pol et al., Structure of ^{22}N and the $N = 14$ subshell. Phys. Rev. C **83**, 064313 (2011). https://doi.org/10.1103/PhysRevC.83.064313
26. S. Bagchi, R. Kanungo, W. Horiuchi et al., Neutron skin and signature of the $N = 14$ shell gap found from measured proton radii of $^{17-22}$N. Phys. Lett. B **790**, 251–256 (2019). https://doi.org/10.1016/j.physletb.2019.01.024
27. Z.H. Yang, Y. Kubota, A. Corsi et al., Quasifree neutron knockout reaction reveals a small s-orbital component in the borromean nucleus ^{17}B. Phys. Rev. Lett. **126**, 082501 (2021). https://doi.org/10.1103/PhysRevLett.126.082501
28. K.J. Cook, T. Nakamura, Y. Kondo et al., Halo structure of the neutron-dripline nucleus ^{19}B. Phys. Rev. Lett. **124**, 212503 (2020). https://doi.org/10.1103/PhysRevLett.124.212503
29. K. Tanaka, T. Yamaguchi, T. Suzuki et al., Observation of a large reaction cross section in the drip-line nucleus ^{22}C. Phys. Rev. Lett. **104**, 062701 (2010). https://doi.org/10.1103/PhysRevLett.104.062701
30. D.Q. Fang, T. Yamaguchi, T. Zheng et al., One-neutron halo structure in ^{15}C. Phys. Rev. C **69**, 034613 (2004). https://doi.org/10.1103/PhysRevC.69.034613
31. R. Kanungo, W. Horiuchi, G. Hagen et al., Proton distribution radii of $^{12-19}$C illuminate features of neutron halos. Phys. Rev. Lett. **117**, 102501 (2016). https://doi.org/10.1103/PhysRevLett.117.102501
32. S. Leblond, F.M. Marqués, J. Gibelin et al., First observation of ^{20}B and ^{21}B. Phys. Rev. Lett. **121**, 262502 (2018). https://doi.org/10.1103/PhysRevLett.121.262502
33. J.G. Li, B.S. Hu, S. Zhang et al., Unbound ^{28}O, the heaviest oxygen isotope observed: a cutting-edge probe for testing nuclear models. Nucl. Sci. Tech. **35**, 21 (2024). https://doi.org/10.1007/s41365-024-01373-w
34. C.X. Yuan, T. Suzuki, T. Otsuka et al., Shell-model study of boron, carbon, nitrogen, and oxygen isotopes with a monopole-based

universal interaction. Phys. Rev. C **85**, 064324 (2012). https://doi.org/10.1103/PhysRevC.85.064324
35. T. Suzuki, R. Fujimoto, T. Otsuka, Gamow-teller transitions and magnetic properties of nuclei and shell evolution. Phys. Rev. C **67**, 044302 (2003). https://doi.org/10.1103/PhysRevC.67.044302
36. T. Suzuki, T. Otsuka, Exotic magnetic properties in ^{17}C. Phys. Rev. C **78**, 061301 (2008). https://doi.org/10.1103/PhysRevC.78.061301
37. Y.F. Geng, J.G. Li, Y.Z. Ma et al., Excitation spectra of the heaviest carbon isotopes investigated within the CD-Bonn Gamow shell model. Phys. Rev. C **106**, 024304 (2022). https://doi.org/10.1103/PhysRevC.106.024304
38. S.J. Dai, F.R. Xu, J.G. Li et al., Continuum effect in resonance spectra of neutron-rich oxygen isotopes. Chinese Phys. C **42**, 114106 (2018). https://doi.org/10.1088/1674-1137/42/11/114106
39. M.R. Xie, J.G. Li, N. Michel et al., Spectroscopic factors of resonance states with the Gamow shell model. Sci. China Phys. Mech. Astron. **67**, 212011 (2023). https://doi.org/10.1007/s11433-023-2227-5
40. G. Thiamova, N. Itagaki, T. Otsuka et al., Systematic analysis of neutron-rich carbon isotopes. Nucl. Phys. A **719**, C312–C315 (2003). https://doi.org/10.1016/S0375-9474(03)00939-4
41. Y. Kanada-En'yo, Proton radii of Be, B, and C isotopes. Phys. Rev. C **91**, 014315 (2015). https://doi.org/10.1103/PhysRevC.91.014315
42. P. Choudhary, P.C. Srivastava, *Ab initio* no-core shell model study of neutron-rich ^{18,19,20}C isotopes. Nucl. Phys. A **1029**, 122565 (2023). https://doi.org/10.1016/j.nuclphysa.2022.122565
43. P. Choudhary, P.C. Srivastava, P. Navrátil, Ab initio no-core shell model study of $^{10-14}$B isotopes with realistic *NN* interactions. Phys. Rev. C **102**, 044309 (2020). https://doi.org/10.1103/PhysRevC.102.044309
44. A. Saxena, P.C. Srivastava, Ab initio no-core shell model study of neutron-rich nitrogen isotopes. Prog. Theor. Exp. Phys. **2019**, 07302 (2019). https://doi.org/10.1093/ptep/ptz073
45. B.R. Barrett, P. Navrátil, J.P. Vary, Ab initio no core shell model. Prog. Part. Nucl. Phys. **69**, 131–181 (2013). https://doi.org/10.1016/j.ppnp.2012.10.003
46. J. Carlson, S. Gandolfi, F. Pederiva et al., Quantum monte carlo methods for nuclear physics. Rev. Mod. Phys. **87**, 1067–1118 (2015). https://doi.org/10.1103/RevModPhys.87.1067
47. G. Hagen, T. Papenbrock, M. Hjorth-Jensen et al., Coupled-cluster computations of atomic nuclei. Rep. Prog. Phys. **77**, 096302 (2014). https://doi.org/10.1088/0034-4885/77/9/096302
48. B.S. Hu, Q. Wu, Z.H. Sun et al., Ab initio Gamow in-medium similarity renormalization group with resonance and continuum. Phys. Rev. C **99**, 061302(R) (2019). https://doi.org/10.1103/PhysRevC.99.061302
49. Q. Yuan, S.Q. Fan, B.S. Hu et al., Deformed in-medium similarity renormalization group. Phys. Rev. C **105**, L061303 (2022). https://doi.org/10.1103/PhysRevC.105.L061303
50. B.S. Hu, W.G. Jiang, T. Miyagi et al., Ab initio predictions link the neutron skin of ^{208}Pb to nuclear forces. Nat. Phys. **18**, 1196 (2022). https://doi.org/10.1038/s41567-022-01715-8
51. J.G. Li, Y.Z. Ma, N. Michel et al., Recent progress in Gamow shell model calculations of drip line nuclei. Physics **3**, 977–997 (2021). https://doi.org/10.3390/physics3040062
52. C. Constantinou, M.A. Caprio, J.P. Vary et al., Natural orbital description of the halo nucleus ^{6}He. Nucl. Sci. Tech. **28**, 179 (2017). https://doi.org/10.1007/s41365-017-0332-6
53. K. Tsukiyama, S.K. Bogner, A. Schwenk, In-medium similarity renormalization group for open-shell nuclei. Phys. Rev. C **85**, 061304 (2012). https://doi.org/10.1103/PhysRevC.85.061304
54. H. Hergert, S.K. Bogner, T.D. Morris et al., The in-medium similarity renormalization group: a novel ab initio method for nuclei. Phys. Rep. **621**, 165–222 (2016). https://doi.org/10.1016/j.physrep.2015.12.007
55. S.R. Stroberg, A. Calci, H. Hergert et al., Nucleus-dependent valence-space approach to nuclear structure. Phys. Rev. Lett. **118**, 032502 (2017). https://doi.org/10.1103/PhysRevLett.118.032502
56. H.H. Li, Q. Yuan, J.G. Li et al., Investigation of isospin-symmetry breaking in mirror energy difference and nuclear mass with ab initio calculations. Phys. Rev. C **107**, 014302 (2023). https://doi.org/10.1103/PhysRevC.107.014302
57. Q. Yuan, B.S. Hu, *Ab initio* calculations of anomalous seniority breaking in the $\pi g_{9/2}$ shell for the N=50 isotones. Phys. Lett. B **858**, 139018 (2024). https://doi.org/10.1016/j.physletb.2024.139018
58. M.R. Xie, L.Y. Shen, J.G. Li et al., *Ab initio* valence-space in-medium similarity renormalization group calculations for neutron-rich P, Cl, and K isotopes*. Chinese Phys. C **48**, 074106 (2024). https://doi.org/10.1088/1674-1137/ad47aa
59. K. Hebeler, S.K. Bogner, R.J. Furnstahl et al., Improved nuclear matter calculations from chiral low-momentum interactions. Phys. Rev. C **83**, 031301 (2011). https://doi.org/10.1103/PhysRevC.83.031301
60. J. Simonis, K. Hebeler, J.D. Holt et al., Exploring *sd*-shell nuclei from two- and three-nucleon interactions with realistic saturation properties. Phys. Rev. C **93**, 011302 (2016). https://doi.org/10.1103/PhysRevC.93.011302
61. V. Somà, P. Navrátil, F. Raimondi et al., Novel chiral Hamiltonian and observables in light and medium-mass nuclei. Phys. Rev. C **101**, 014318 (2020). https://doi.org/10.1103/PhysRevC.101.014318
62. P. Gysbers, G. Hagen, J.D. Holt et al., Discrepancy between experimental and theoretical β-decay rates resolved from first principles. Nat. Phys. **15**, 428–431 (2019). https://doi.org/10.1038/s41567-019-0450-7
63. R. Roth, S. Binder, K. Vobig et al., Medium-mass nuclei with normal-ordered chiral *NN*+3*N* interactions. Phys. Rev. Lett. **109**, 052501 (2012). https://doi.org/10.1103/PhysRevLett.109.052501
64. T.D. Morris, N.M. Parzuchowski, S.K. Bogner, Magnus expansion and in-medium similarity renormalization group. Phys. Rev. C **92**, 034331 (2015). https://doi.org/10.1103/PhysRevC.92.034331
65. N. Shimizu, T. Mizusaki, Y. Utsuno et al., Thick-restart block lanczos method for large-scale shell-model calculations. Comput. Phys. Commun. **244**, 372–384 (2019). https://doi.org/10.1016/j.cpc.2019.06.011
66. https://www.nndc.bnl.gov/ensdf/
67. M.D. Jones, T. Baumann, J. Brett et al., Neutron-unbound excited states of ^{23}N. Phys. Rev. C **95**, 044323 (2017). https://doi.org/10.1103/PhysRevC.95.044323
68. L. Zhou, D.Q. Fang, S.M. Wang et al., Structure and 2p decay mechanism of ^{18}Mg. Nucl. Sci. Tech. **35**, 107 (2024). https://doi.org/10.1007/s41365-024-01479-1
69. A. Spyrou, T. Baumann, D. Bazin et al., First evidence for a virtual ^{18}B ground state. Phys. Lett. B **683**, 129–133 (2010). https://doi.org/10.1016/j.physletb.2009.12.016
70. T. Otsuka, R. Fujimoto, Y. Utsuno et al., Magic numbers in exotic nuclei and spin-isospin properties of the *N N* interaction. Phys. Rev. Lett. **87**, 082502 (2001). https://doi.org/10.1103/PhysRevLett.87.082502
71. Y.Z. Ma, L. Coraggio, L. De Angelis et al., Contribution of chiral three-body forces to the monopole component of the effective

shell-model Hamiltonian. Phys. Rev. C **100**, 034324 (2019). https://doi.org/10.1103/PhysRevC.100.034324

72. J. Elliott, A. Jackson, H. Mavromatis et al., Matrix elements of the nucleon-nucleon potential for use in nuclear-structure calculations. Nucl. Phys. A **121**, 241–278 (1968). https://doi.org/10.1016/0375-9474(68)90419-3
73. M.W. Kirson, Spin-tensor decomposition of nuclear effective interactions. Phys. Lett. B **47**, 110–114 (1973). https://doi.org/10.1016/0370-2693(73)90582-0
74. A. Umeya, K. Muto, Single-particle energies in neutron-rich nuclei by shell model sum rule. Phys. Rev. C **74**, 034330 (2006). https://doi.org/10.1103/PhysRevC.74.034330